

# Low Dissipation Simulation for Vortex Flowfield of Rotor in Hover Based upon Discontinuous Galerkin Method

BIAN Wei<sup>1</sup>, ZHAO Qijun<sup>1\*</sup>, ZHAO Guoqing<sup>1,2</sup>

1. National Key Laboratory of Rotorcraft Aeromechanics, College of Aerospace Engineering, Nanjing University of Aeronautics and Astronautics, Nanjing 210016, P.R. China;

2. Rotor Aerodynamic Key Laboratory, China Aerodynamic Research and Development Center, Mianyang 621000, P.R. China

(Received 1 October 2020; revised 15 September 2021; accepted 20 October 2021)

**Abstract:** The discontinuous Galerkin (DG) method is established and innovatively conducted on accurately simulating the evolution of blade-tip vortex and the aerodynamic characteristics of helicopter rotor. Firstly, the Reynolds-Averaged Navier-Stokes (RANS) equations in rotating reference frame are employed, and the embedded grid system is developed with the finite volume method (FVM) and the DG method conducted on the blade grid and background grid respectively. Besides, the Harten-Lax-Van Leer contact (HLLC) scheme with high-resolution and low-dissipation is employed for spatial discretization, and the explicit third-order Runge-Kutta scheme is used to accomplish the temporal discretization. Secondly, the aerodynamic characteristics and the evolution of blade-tip vortex for Caradonna-Tung rotor are simulated by the established CFD method, and the numerical results are in good agreement with experimental data, which well validates the accuracy of the DG method and shows the advantages of DG method on capturing the detailed blade-tip vortex compared with the FVM method. Finally, the evolution of tip vortex at different blade tip Mach numbers and collective pitches is discussed.

**Key words:** blade-tip vortex; discontinuous Galerkin (DG) method; Navier-Stokes (N-S) equations; aerodynamic characteristics; helicopter rotor

**CLC number:** V211.52

**Document code:** A

**Article ID:** 1005-1120(2021)06-0975-09

## 0 Introduction

Intense vortices form at blade tips with the rotation of the helicopter rotor, and as the rolling up and shedding of vortices, the flowfield of rotor is dominated by the vortex wake. Therefore, helicopters are manipulated in the environment of rotor vortex flowfield, and the blade-tip vortex shedding from the front blade might strike on rear blade which causes strong blade vortex interaction (BVI). Moreover, the blade-tip vortex falling downward and backward will impact the surface of fuselage and tail rotor and other parts of helicopter, resulting in serious aerodynamic interactions<sup>[1]</sup>. These phenomena will seriously affect the aerodynamic performance of the rotor, and cause the reduction of aerodynamic

performance of fuselage and tail rotor. So it has theoretical and practical value to simulate the evolution of blade-tip vortex, which will further help analyze the aerodynamic characteristics of helicopter.

A lot of studies on the evolution of blade-tip vortex have been carried out. Previously, most of the researches on blade-tip vortex were carried out through experiment. In 2000, Heineck et al.<sup>[2]</sup> acquired the velocity fields for wake ages ranging from 0° to 270° in hover by particle image velocimetry (PIV) technique, and the experiment represented a major step toward understanding the detailed structure of a rotor wake. Martin et al.<sup>[3]</sup> further tested the blade-tip vortex by PIV and laser Doppler velocimetry (LDV) equipment. It can be found by con-

\*Corresponding author, E-mail address: zhaqijun@nuaa.edu.cn.

**How to cite this article:** BIAN Wei, ZHAO Qijun, ZHAO Guoqing. Low dissipation simulation for vortex flowfield of rotor in hover based upon discontinuous Galerkin method[J]. Transactions of Nanjing University of Aeronautics and Astronautics, 2021, 38(6):975-983.

<http://dx.doi.org/10.16356/j.1005-1120.2021.06.008>

trast that PIV is much faster than LDV and has the advantage of being a whole-plane measurement technique. However, PIV is more sensitive to calibration errors and can suffer from spatial resolution issues if large regions of the flow are to be interrogated<sup>[4]</sup>. In addition, the whole process of experiment has a long period and high cost including model design, rotor manufacturing, test preparation, measurement process and data process. Compared with the experiment, the CFD method can quickly and fully capture the rotor flowfield for blades with different shapes, considering the viscosity and compressibility of the air, which makes up for the deficiency of the experiment.

The previous CFD methods<sup>[5-7]</sup>, such as the small disturbance equation and the full potential equation, are restricted by the irrotational, inviscid and isentropic assumptions, which cannot obtain the information of the vortex field. With the improvement of computing capability, the numerical simulation method of rotor in hover based on Euler equations and Navie-Stokes equations has gradually matured. Srinivasan and Baeder<sup>[8]</sup> employed the N-S equations based on the Roe scheme without specifying any wake models to establish a CFD method for solving the flowfield of rotor in hover. The analyzed aerodynamic performance of rotor is in good agreement with the experimental data, but it is difficult to capture blade-tip vortex with large velocity gradient due to the coarse grids and excessive numerical dissipation. In order to reduce the numerical dissipation, some researchers have proposed high-order numerical methods to improve the ability to capture the tip vortex of the rotor. Zhao et al.<sup>[9]</sup> established a rotor flowfield code based on the Roe scheme and third-order monotone upstream-centred schemes for conservation law (MUSCL) scheme. Hariharan<sup>[10]</sup> introduced a high-order weighted essentially non-oscillatory (WENO) scheme to effectively capture the blade-tip vortex. After that, different high-order numerical methods were successively developed to simulate the flowfield<sup>[11]</sup>. Finite volume method (FVM) is mainly used for the flowfield simulation of rotor at present, and most of FV methods improve the numerical accuracy by extending sten-

cils<sup>[12]</sup>, which is difficult to choose the stencils to computer the derivatives in practice for unstructured grids. Unlike the FV methods, where the derivatives are reconstructed using the mean values of neighboring cells, the discontinuous Galerkin (DG) method<sup>[13]</sup> solves the equations for the derivatives in a manner similar to the mean variables and provides a unified formulation to represent the numerical polynomial solutions in each element, which reduces the numerical dissipation in the simulation, and has a great advantage in simulating the evolution of the blade-tip vortex.

It is easy to construct arbitrary order polynomials to improve the accuracy of numerical simulations and enhance the capture of flow details by employing the DG method. Besides, it is compact and each element is independent in DG method, so it can be highly parallelizable which could help to improve the efficiency of numerical method. Luo et al.<sup>[14]</sup> applied the DG method based on the Taylor series expansion to simulate the classical flow around the cylinder and the two-dimensional steady state airfoil flowfield, and the calculated results are in good agreement with the experimental data. Then, the ONE-RA M6 Wing<sup>[15]</sup> is numerically simulated, the pressure coefficient distribution is very close to the experimental values and more details of the flowfield are captured. At present, the DG method is mostly used in the numerical simulation of the two-dimensional flowfield and the three-dimensional fixed-wing flowfield<sup>[16-18]</sup>, and has not yet simulated the flowfield of the rotating rotor. In order to improve the accuracy of capturing the tip vortex of the rotor, the numerical simulation of rotor flowfield based on DG method has good academic value.

In this paper, the DG method is established and innovatively conducted on accurately simulating the evolution of blade-tip vortex and the aerodynamic characteristics of helicopter rotor. Embedded grid technology is adopted and blade grid with good orthogonality is generated and appropriately refined based on Poisson equations. The finite volume method is used to numerically simulate the flowfield of the blade grid. In order to reduce the numerical dissipation of the background grid, the DG method

is used to simulate the evolution of the blade-tip vortex. The blade-tip vortex in hover is numerically simulated using the established method and the parameterized calculation of Caradonna-Tung (C-T) rotor is carried out with different blade-tip Mach numbers and collective pitches.

## 1 Computational Methods

### 1.1 Embedded grid methodology

Embedded grid methodology<sup>[19]</sup> is adopted to discretize the calculation domain of rotor flowfield in which O—C—O type body-fitted grid is generated around rotor blade, and the cylindrical Cartesian grid is adopted for the background grid<sup>[9]</sup>. Fig.1 shows the the whole embedded grid system.

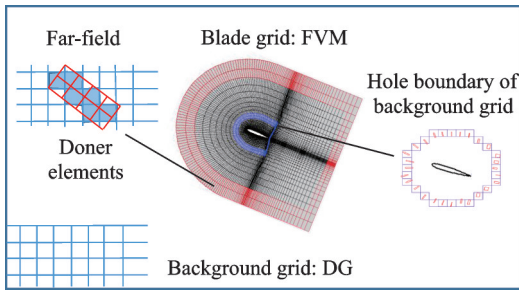


Fig.1 Embedded grid system around rotor

FVM is conducted on the blade grid. In order to reduce the numerical dissipation and capture more revolutions of tip vortex with minimal diffusion, the DG method is conducted on the background grid which is dominated by the vortex wake. Considering that the viscous effects on background grid have little influence on the revolution of rotor flowfield, the background grid away from the rotor surface is treated as inviscid in order to reduce the calculation consumption.

### 1.2 Governing equations

The Navier-Stokes equations in rotating reference frame are employed as governing equations for simulating the quasi-steady flowfield of rotor in hover, and the expression is

$$\frac{\partial}{\partial t} \int_V U dV + \int_S (F_c^i - F_v^i) \cdot n dS = \int_V Q dV \quad (1)$$

where  $U$  is the conservation variable, considering the contravariant velocity  $-\Omega$  of cell surface and

original convective flux  $F_{c0}^i$ ,  $F_c^i$  the modified convective flux vector,  $F_v^i$  the viscous flux vector,  $Q$  the source term,  $S$  the boundary of  $V$ , and  $n$  the unit outward normal vector to the boundary, which can be written as

$$U = \begin{pmatrix} \rho \\ \rho u_1 \\ \rho u_2 \\ \rho u_3 \\ \rho E \end{pmatrix}, Q = \begin{pmatrix} 0 \\ -\rho \Omega u_3 \\ 0 \\ \rho \Omega u_1 \\ 0 \end{pmatrix}, F_v^i = \begin{pmatrix} 0 \\ \tau_{1i} \\ \tau_{2i} \\ \tau_{3i} \\ \Theta_i \end{pmatrix} \quad (2)$$

$$F_c^i = F_{c0}^i - (-\Omega U) = \begin{pmatrix} \rho u_i - \rho u_{ii} \\ \rho u_1 u_i + p \delta_{1i} - \rho u_1 u_{ii} \\ \rho u_2 u_i + p \delta_{2i} - \rho u_2 u_{ii} \\ \rho u_3 u_i + p \delta_{3i} - \rho u_3 u_{ii} \\ \rho u_i h - \rho E u_{ii} \end{pmatrix} \quad (3)$$

where  $\rho$ ,  $p$ ,  $E$  and  $h$  denote the density, pressure, specific total energy and the specific total enthalpy of the fluid, respectively.  $u_i$  is the velocity of the flow in the coordinate direction,  $\Omega$  the rotating angular velocity of the rotor,  $\tau$  the viscous stress tensor,  $u_{ii}$  the rotating velocity of rotor in the coordinate direction,  $\Theta$  the work of viscous stresses and heat conduction in the fluid, and  $\delta_{ij}$  the Kronecker delta function.

Aimed at well simulating separated airflow over surface of rotor, one-equation Spalart-Allmaras (S-A)<sup>[20]</sup> model is used to simulate turbulent flows.

### 1.3 DG method

#### 1.3.1 DG method on background grid

Euler equations are employed as governing equations on background grid and the governing equations are discretized using a DG formulation. Firstly, the following weak formulation is introduced, which is obtained by multiplying the above conservation law by a test function  $W$ , integrating over the domain  $V$ , and performing an integration by parts

$$\frac{\partial}{\partial t} \int_V U W dV + \int_S F_c \cdot n W dS - \int_V F_c \frac{\partial W}{\partial x_i} dV = \int_V Q W dV \quad (4)$$

Assume that the domain  $V$  is subdivided into a collection of non-overlapping elements  $\Omega_e$ . Then, the broken Sobolev space  $V_h^p$  consists of discontinu-

ous vector-values polynomial functions of degree  $p$  is as follows

$$V_h^p = \left\{ v_h \in [L_2(V)]^m : v_h|_{\Omega_e} \in [V_p^m] \quad \forall \Omega_e \in V \right\} \quad (5)$$

where  $m$  is the dimension of conservative state vector, and the Sobolev space can be written as

$$V_h^p = \text{span} \left\{ \prod_{i=1}^d x_i^{\alpha_i} : 0 \leq \alpha \leq p, 0 \leq i \leq d \right\} \quad (6)$$

where  $\alpha$  denotes a multi-index and  $d$  the dimension of space. After that, the following semi-discrete form by applying the weak formulation on each element  $\Omega_e$  can be obtained as

$$\begin{aligned} \frac{d}{dt} \int_{\Omega_e} \mathbf{U}_h \mathbf{W}_h dV + \int_{\Gamma_e} \mathbf{F}_c(\mathbf{U}_h) \cdot \mathbf{n} \mathbf{W}_h dS - \\ \int_{\Omega_e} \mathbf{F}_c(\mathbf{U}_h) \frac{\partial \mathbf{W}_h}{\partial x_i} dV = \int_{\Omega_e} \mathbf{Q} \mathbf{W}_h dV \end{aligned} \quad (7)$$

where  $\mathbf{U}_h$  and  $\mathbf{W}_h$  denote the finite element approximations to the analytical solution  $\mathbf{U}$  and the test function  $\mathbf{W}$ , respectively. Assume that  $B$  is the basis of polynomial function of degree  $p$ , then the system of  $N$  equations can be achieved as

$$\begin{aligned} \frac{d}{dt} \int_{\Omega_e} \mathbf{U}_h B_i dV + \int_{\Gamma_e} \mathbf{F}_c(\mathbf{U}_h) \cdot \mathbf{n} B_i dS - \\ \int_{\Omega_e} \mathbf{F}_c(\mathbf{U}_h) \frac{\partial B_i}{\partial x_j} dV = \int_{\Omega_e} \mathbf{Q} B_i dV \quad 1 \leq i \leq N \end{aligned} \quad (8)$$

where  $N$  denotes the dimension of the polynomial space. A Taylor series expansion at the centroid of the cell is adopted to represent the numerical polynomials solutions in each element, and the polynomial solutions can be expressed as

$$\mathbf{U}_h = \bar{\mathbf{U}} B_1 + \frac{\partial \mathbf{U}}{\partial x} \Delta x B_2 + \frac{\partial \mathbf{U}}{\partial y} \Delta y B_3 + \frac{\partial \mathbf{U}}{\partial z} \Delta z B_4 \quad (9)$$

where  $B_1 = 1$ ,  $B_2 = \frac{x - x_c}{\Delta x}$ ,  $B_3 = \frac{y - y_c}{\Delta y}$ ,  $B_4 = \frac{z - z_c}{\Delta z}$ ,  $\bar{\mathbf{U}}$  denotes the mean value in the cell,  $(x_c, y_c, z_c)$  the centroid of the cell, and  $(\Delta x, \Delta y, \Delta z)$  the cell size.

In this paper, the Harten-Lax-Van Leer contact (HLLC)<sup>[21]</sup> approximate Riemann solver is adopted for the inviscid flux spatial discretization, which is applicable to both structured and unstructured grids and has low storage requirements. Gaussian integration quadrature formula is employed in discontinuous finite element calculations since they present the best accuracy for a given num-

ber of points. The HLLC flux is defined by

$$H_{\text{HLLC}}(\mathbf{U}_l, \mathbf{U}_r, n_{ij}) = \begin{cases} H_1(\mathbf{U}_l) & S_L > 0 \\ H(\mathbf{U}_1^*) & S_L \leq 0 < S_M \\ H(\mathbf{U}_r^*) & S_M \leq 0 \leq S_R \\ H_r(\mathbf{U}_r) & S_R < 0 \end{cases} \quad (10)$$

where  $\mathbf{U}_l$  and  $\mathbf{U}_r$  are the solution polynomials at the left and right states of the cell interface.

### 1.3.2 Time integration

In this paper, the explicit method is employed in the temporal discretization of the semi-discrete system. Here, the explicit three-stage third-order TVD Runge-Kutta scheme<sup>[22]</sup> is adopted

$$\begin{cases} \mathbf{U}^{(1)} = \mathbf{U}^n + \Delta t \mathbf{M}^{-1} \mathbf{R}(\mathbf{U}^n) \\ \mathbf{U}^{(2)} = \frac{3}{4} \mathbf{U}^n + \frac{1}{4} [\mathbf{U}^{(1)} + \Delta t \mathbf{M}^{-1} \mathbf{R}(\mathbf{U}^{(1)})] \\ \mathbf{U}^{n+1} = \frac{1}{3} \mathbf{U}^n + \frac{2}{3} [\mathbf{U}^{(2)} + \Delta t \mathbf{M}^{-1} \mathbf{R}(\mathbf{U}^{(2)})] \end{cases} \quad (11)$$

where  $\mathbf{M}$  denotes the mass matrix and it has the block diagonal structure.  $\mathbf{R}(\mathbf{U})$  is the residual vector obtained by flux calculation.

$$\mathbf{M} = \begin{bmatrix} m & 0 & 0 & 0 & 0 \\ 0 & m & 0 & 0 & 0 \\ 0 & 0 & m & 0 & 0 \\ 0 & 0 & 0 & m & 0 \\ 0 & 0 & 0 & 0 & m \end{bmatrix} \quad (12)$$

$$\mathbf{m} = \begin{bmatrix} V & 0 & 0 & 0 \\ 0 & \int_{\Omega_e} B_2 B_2 d\Omega & \int_{\Omega_e} B_2 B_3 d\Omega & \int_{\Omega_e} B_2 B_4 d\Omega \\ 0 & \int_{\Omega_e} B_3 B_2 d\Omega & \int_{\Omega_e} B_3 B_3 d\Omega & \int_{\Omega_e} B_3 B_4 d\Omega \\ 0 & \int_{\Omega_e} B_4 B_2 d\Omega & \int_{\Omega_e} B_4 B_3 d\Omega & \int_{\Omega_e} B_4 B_4 d\Omega \end{bmatrix} \quad (13)$$

### 1.3.3 Information transmission

The flowfield information of the contributing element of background grid needs to be transferred to the corresponding outer boundary grid of the blade. Because the DG method used in the background grid obtains high-order accuracy by polynomial interpolation in the element, which can calculate the conservative variables accurately at a certain point, it is more accurate when transmitting information to the blade grid. As shown in Fig.2, element  $A$  is an outer boundary grid of the blade, and the center point of the element falls on element  $B$  of the background grid. On the background grid, the mean value and the partial derivative of the conservative variables

are used to calculate the actual value at point  $a$  which is transferred to element  $A$  of the blade grid.

The specific formula is as follows

$$U_a = \bar{U}_B B_1 + \frac{\partial U_B}{\partial x} \Delta x B_2 + \frac{\partial U_B}{\partial y} \Delta y B_3 + \frac{\partial U_B}{\partial z} \Delta z B_4 \quad (14)$$

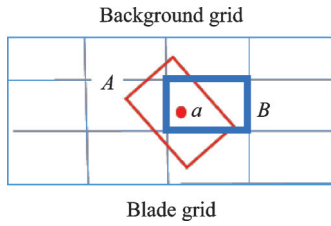


Fig.2 Schematic diagram of value transfer from background grid to blade grid

## 2 Numerical Examples

### 2.1 Validation of CFD method

The classic C-T rotor<sup>[23]</sup> is taken as validation case for simulation of aerodynamic characteristics of rotor. The rotor has two rectangular blades with aspect ratio of 6. NACA0012 airfoil is adopted in the rotor blade without twist. The hover condition with a collective pitch of  $8^\circ$ , and blade-tip Mach number  $Ma_{tip} = 0.439$  is conducted for numerical simulation. The number of grids around the blade is  $213 \times 49 \times 110$ , and the number of background grids is  $121 \times 150 \times 120$ .

Fig.3 shows the calculated and experimental pressure coefficient ( $C_p$ ) distribution of several sections. In Fig.3,  $x/c$  is the chord position of the blade, and  $r/R$  is the radial position of the blade section. It can be seen that the pressure coefficient distribution calculated by the method used in this paper is in good agreement with the experimental data in each section of the rotor blade, which shows the effectiveness of the method in this paper.

In order to capture the evolution process of blade-tip vortex better, the effects of special blade-tip shape and twist distribution should be excluded. Therefore, the C-T model rotor is chosen to be simulated. The Jameson scheme, the fifth-order Roe-WENO scheme and the method established in this paper are used to simulate the hover condition re-

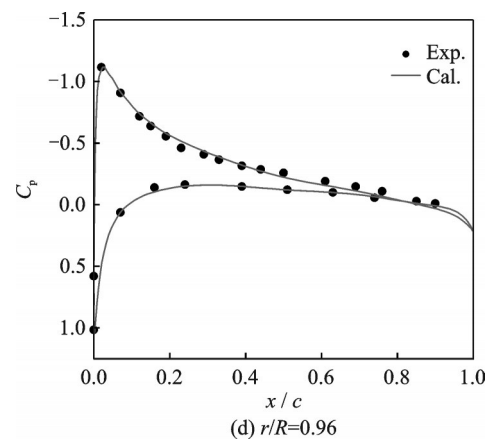
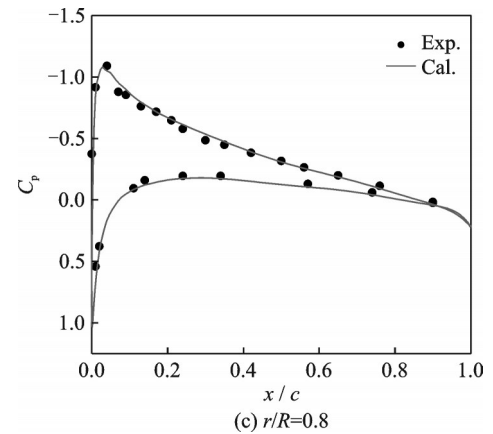
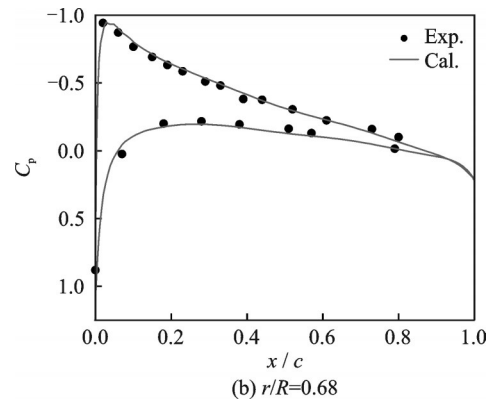
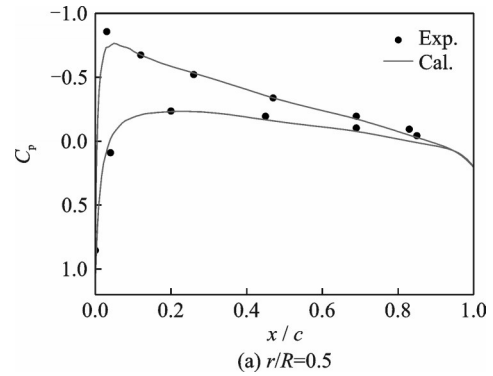


Fig.3 Comparison of pressure coefficient distribution at different sections of C-T rotor ( $Ma_{tip} = 0.439$ )

spectively. The background grid is properly refined in order to capture more revolutions of the blade-tip vortex, and the number of grids around the blade is  $259 \times 49 \times 180$ , and the number of background grids is  $151 \times 253 \times 160$ . Table 1 shows the rotor thrust coefficient calculated by three different methods respectively. It can be seen that thrust coefficient calculated by the method adopted in this paper is more comparable to the experimental data, which illustrates the accuracy of the calculation of the aerodynamic performance of the rotor, and the error of thrust coefficient is less than 4%.

**Table 1 Aerodynamic performance comparison between different methods**

Scheme	$C_T/10^{-3}$	Error/%
Jameson	4.810 8	4.81
Roe+WENO	4.793 9	4.44
DG+HLLC	4.735 9	3.17
Experimental value	4.590 0	

The vorticity iso-surfaces of C-T rotor at the collective pitch angle of  $8^\circ$  are shown in Fig.4. It can be seen that the blade-tip vortex simulated by Jameson-Schmidt-Turkel (JST) scheme is not complete, and the vortex sheds about  $360^\circ$  until it dissipates completely. The wake age captured by fifth-order Roe-WENO scheme can reach  $720^\circ$ . On the contrary, the blade-tip vortex simulated by the method established in this paper sustains to more than  $800^\circ$  before it dissipates completely. Fig.5 shows the vorticity iso-surfaces on the section simulated by the JST scheme and the DG method, respectively. The same grids are adopted in three different methods, which indicates the ability of Discontinuous Galerkin method used in this paper to reduce the numerical dissipation. It can be found that the method established in this paper could simulate the vortex flowfield of the rotor more accurately through the



Fig.4 Comparisons of vorticity iso-surfaces among different methods

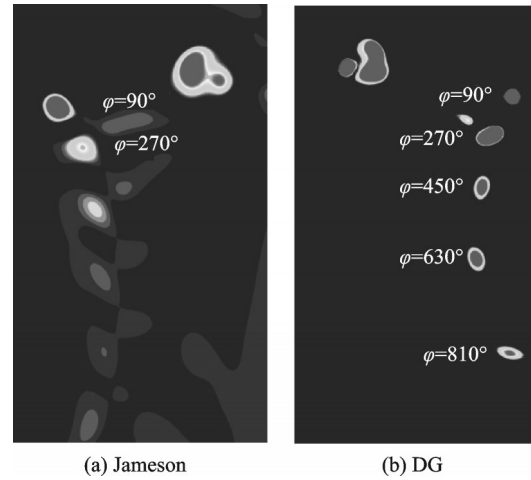


Fig.5 Comparison of vorticity iso-surfaces

comparison.

Figs.6(a, b) show the predicted trajectories of the blade-tip vortex in vertical and radial directions respectively, where  $y/R$ ,  $r/R$  denote the vertical position and the radial position, and  $\varphi$  is the wake age. It can be seen that the vertical and radial displacements of blade-tip vortex simulated by the method established in this paper are in good agree-

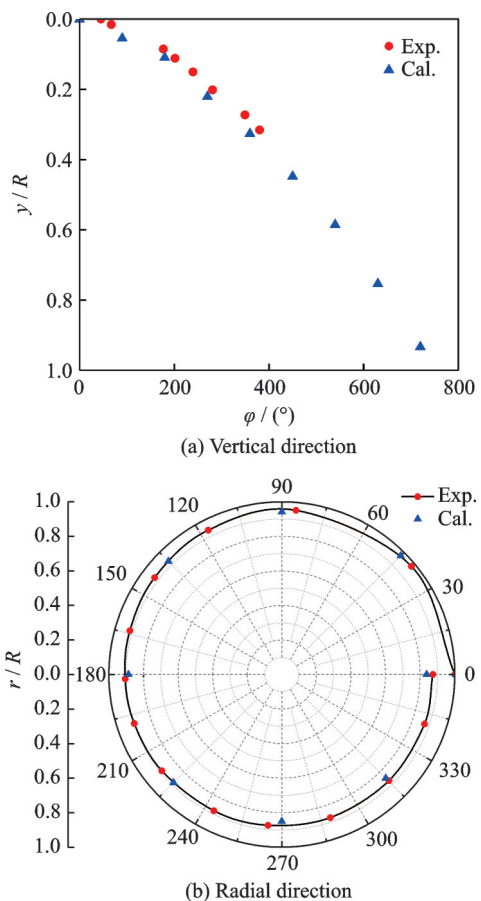


Fig.6 Blade-tip vortex location of C-T rotor

ment with the experimental data for a wake age up to  $360^\circ$ .

Fig.7 shows the vorticity iso-surfaces on two typical circumferential sections where the wake age between the sections differs by  $90^\circ$ . It can be seen from Fig.6 and Fig.7 that the blade-tip vortex will be contracted to the root of the blade when it develops downstream along the vertical direction and the contraction degree of the blade-tip vortex will be slowed down when wake age is greater than  $360^\circ$ , then, the tip vortex begins to expand outward. With the increase of wake age, the vorticity value of blade-tip vortex continues to decrease, resulting from physical dissipation and numerical dissipation. When the blade-tip vortex develops downward to a certain extent, the vertical speed of vortex-core motion increases. This sudden increase in downward convection is the result of the downwash from the blade and the evolving tip vortex on the first passage of the vortex. The dissipation of vortex continues to increase until the blade-tip vortex dissipates completely.

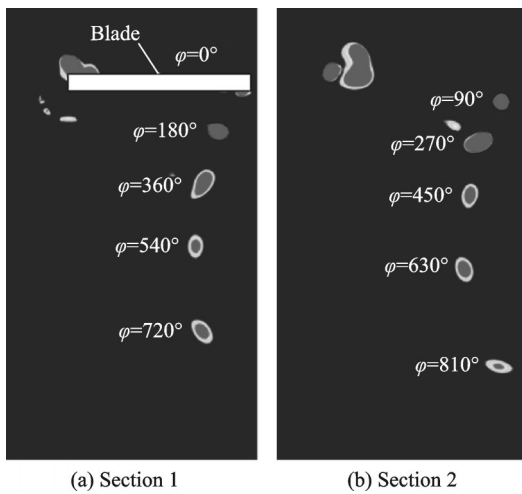


Fig.7 Vorticity iso-surfaces of different sections

## 2.2 Analysis on evolution of blade-tip vortex

In order to study the evolution of the blade-tip vortex of the rotor, the parameterized calculation of C-T rotor is carried out at different blade tip Mach numbers and collective pitches. Mach number ranges from 0.439 to 0.794, and collective pitch of rotor ranges from  $5^\circ$  to  $9^\circ$ .

Fig.8 shows the vertical position  $y/R$  and the

radial position  $r/R$  of the C-T rotor tip vortex core with a collective pitch of  $8^\circ$  and blade tip Mach numbers are 0.439, 0.526, 0.612, 0.727 and 0.794, respectively. It can be seen from Fig.8 (a) that the larger the Mach number is, the slower the vertical descent speed of the vortex will be. It can be seen from Fig.8(b) that the larger the Mach number is, the larger the wake age at which the tip vortex begins to expand outward is, and its contraction speed is relatively slow.

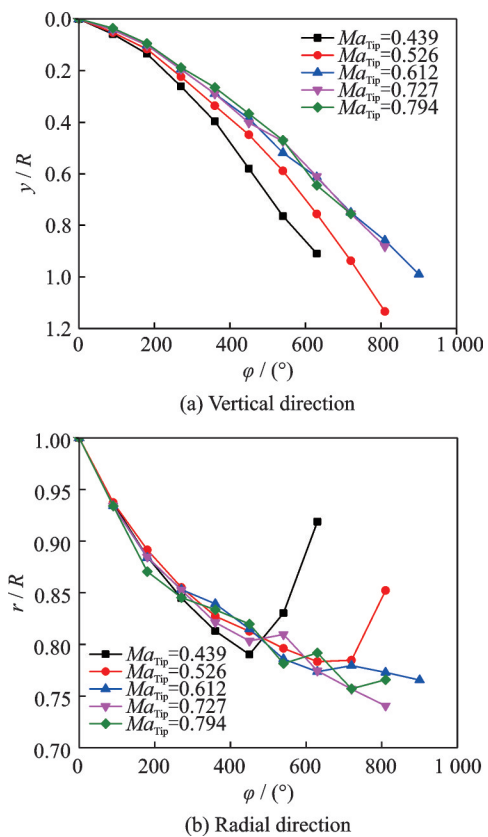


Fig.8 Blade-tip vortex location at different blade-tip Mach numbers

Fig.9 shows the vertical position and radial position of the C-T rotor tip vortex core with the blade tip Mach number is 0.794 and the collective pitches are  $5^\circ$ ,  $6^\circ$ ,  $7^\circ$ ,  $8^\circ$ , and  $9^\circ$ , respectively. In Fig.9 (a), the greater the collective pitch is, the stronger the downwash induced by the rotor is, and the faster the vertical descent speed is. It can be seen from Fig.9(b) that the collective pitch has little influence on the radial motion of the blade-tip vortex. Similarly, the wake age reaching the contraction limit is little affected by the collective pitch of rotor.

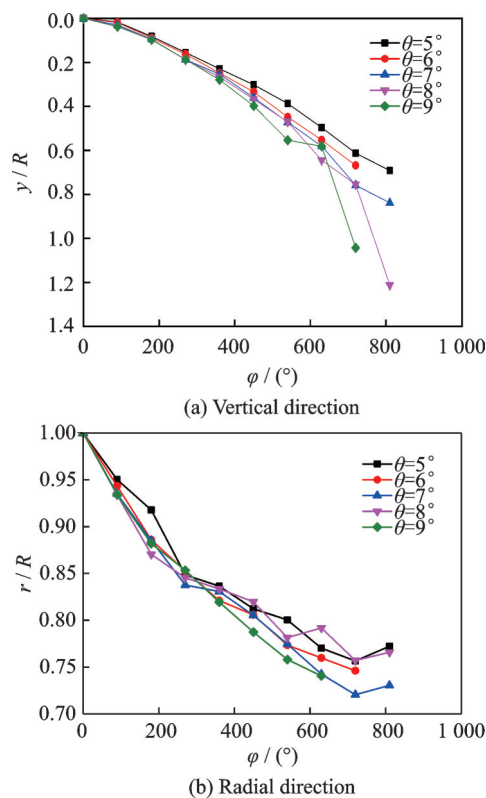


Fig.9 Blade-tip vortex location at different collective pitches

### 3 Conclusions

A numerical simulation method based on the DG method has been developed for the prediction of rotor flowfield in hover in this paper. The aerodynamic performance and evolution of the blade-tip vortex of C-T rotor are simulated and analyzed by the established method, and the following conclusions can be obtained:

(1) The pressure coefficient distribution calculated by the method established in this paper is in good agreement with the experimental data, and the error of the thrust coefficient is less than 4%.

(2) The comparison of the simulated results indicates that the DG method has the characteristic of lower numerical dissipation compared with the JST scheme and the Roe-WENO scheme, and it could predict the characteristics of blade-tip vortex more accurately.

(3) There is a contraction limit during the downward development of blade-tip vortex. After the limited position, the tip vortex begins to expand outward and the speed of vortex-core motion increases. The dissipation of vortex continues to increase until the blade-tip vortex dissipates completely.

### References

- [1] YE Z, XU G H, SHI Y J. Computational research on aerodynamic characteristics of helicopter main-rotor/tail rotor/vertical-tail interaction[J]. *Acta Aeronautica et Astronautica Sinica*, 2015, 36(9): 2874-2883.
- [2] HEINECK J T, YAMAUCHI G K. Application of three-component PIV to a hovering rotor wake[C]// *Proceedings of the 56th AHS Annual Forum*. Fairfax Virginia: American Helicopter Society, 2000.
- [3] MARTIN P B, LEISHMAN J G. Stereoscopic PIV measurements in the wake of a hovering rotor[C]// *Proceedings of the 56th AHS Annual Forum*. Fairfax Virginia: American Helicopter Society, 2000.
- [4] DURAISAMY K, RAMASAMY M, BAEDER J D, et al. High-resolution computational and experimental study of rotary-wing tip vortex formation[J]. *AIAA Journal*, 2007, 45(11): 2593-2602.
- [5] LANDEGREBE A J, CHENEY M C. Rotor wakes—Key to performance prediction[C]// *Proceedings of AGARD Conference on Aerodynamics of Rotary Wings*. [S.l.]: AGARD, 1973.
- [6] BEDDOES T S. A wake model for high resolution airloads[C]// *Proceedings of the 2nd International Conference on Basic Rotorcraft Research*. [S.l.]: [s.n.], 1985.
- [7] SANKAR L N, MALONE J B. A strongly implicit procedure for steady three dimensional transonic potential flow[J]. *AIAA Journal*, 1982, 20(5): 598-605.
- [8] SRINIVASAN G R, BAEDER J D. Flowfield of a lifting rotor in hover—A Navier-Stokes simulation[J]. *AIAA Journal*, 1992, 30(10): 2371-2378.
- [9] ZHAO Q J, ZHAO G Q, WANG B, et al. Robust navier-stokes method for predicting unsteady flowfield and aerodynamic characteristics of helicopter rotor[J]. *Chinese Journal of Aeronautics*, 2018, 31(2): 214-224.
- [10] HARIHARAN N. Rotary-wing wake capturing: High order schemes towards minimizing numerical vortex dissipation[J]. *AIAA Journal of Aircraft*, 2002, 39(5): 822-830.
- [11] SANKARAN V, SITARAMAN J, WISSINK A, et al. Application of the Helios computational platform to rotorcraft flowfields [C]// *Proceedings of the 48th AIAA Aerospace Sciences Meeting Including the New Horizons Forum and Aerospace Exposition*. Orlando, Florida: AIAA, 2010.
- [12] SITARAMAN J, POTSDAM M. Rotor loads prediction using Helios: A multisolver framework for rotorcraft aeromechanics analysis[J]. *Journal of Aircraft*, 2013, 50(2): 478-493.
- [13] REED W H, HILL T R. Triangular mesh methods for the neutron transport equation: LA-UR-73-

- 479[R]. New Mexico, USA: Los Alamos Scientific Laboratory, 1973.
- [14] LUO H, BAUM J D. A discontinuous Galerkin method based on a Taylor basis for the compressible flows on arbitrary grids[J]. Journal of Computational Physics, 2008, 227(20): 8875-8893.
- [15] LUO H, XIA Y, LI S, et al. A hermite WENO reconstruction-based discontinuous Galerkin method for the euler equations on tetrahedral grids[J]. Journal of Computational Physics, 2012, 231(16): 5489-5503.
- [16] ZHANG Tao, LYU Hongqiang, QIN Wanglong, et al. Numerical simulations of turbulent flow based on rotating reference frame using high-order discontinuous Galerkin method[J]. Journal of Nanjing University of Aeronautics & Astronautics, 2019, 51(4): 474-482. (in Chinese)
- [17] YANG X Q, CHENG J, LUO H. Robust implicit direct discontinuous Galerkin method for simulating the compressible turbulent flows[J]. AIAA Journal, 2018, 57(3): 1-20.
- [18] YANG X Q, CHENG J, LUO H. A reconstructed direct discontinuous Galerkin method for simulating the compressible laminar and turbulent flows on hybrid grids[J]. Computers & Fluids, 2018, 168: 216-231.
- [19] CHIU T, MEAKIN R L. On automating domain connectivity for overset grids: AIAA-1995-0854[R]. Reston: AIAA, 1995.
- [20] SPALART P R, ALLMARAS S R. A one-equation turbulence model for aerodynamic flows[C]//Proceedings of the 30th Aerospace Sciences Meeting and Exhibit.[S.l.]: AIAA, 1992.
- [21] BATTEN P, LESCHZINER M A, GOLDBERG U C. Average-state Jacobians and implicit methods for compressible viscous and turbulent flows[J]. Journal of Computational Physics, 1997, 137(1): 38-78.
- [22] ATKINS H L, SHU C W. Quadrature-free implementation of the discontinuous Galerkin method for hyperbolic equations[J]. AIAA Journal, 1996, 36(5): 775-782.
- [23] CARADONNA F X, TUNG C. Experimental and analytical studies of a model helicopter rotor in hover[J]. Vertica, 1981, 5(1): 149-161.

**Acknowledgements** This work was supported by the National Natural Science Foundation of China (Nos.12072156, 12032012), the Foundation of Rotor Aerodynamic Key Laboratory (No.RAL20190102), and the Priority Academic Program Development Project of Jiangsu Higher Education Institutions (PAPD).

**Authors** Mr. BIAN Wei is a Ph.D. candidate at Nanjing University of Aeronautics and Astronautics (NUAA). His research domain is high precision CFD method of helicopter aerodynamic characteristics.

Prof. ZHAO Qijun received his Ph.D. degree from NUAA in 2005. His research interests are helicopter aerodynamics, computational fluid dynamics of rotor, aeroacoustic noise of rotors, and active flow control, etc.

**Author contributions** Prof. ZHAO Qijun designed the whole study. Mr. BIAN Wei wrote the manuscript. Dr. ZHAO Guoqing performed the simulation and analyzed the results. All authors commented on the manuscript draft and approved the submission.

**Competing interests** The authors declare no competing interests.

(Production Editor: SUN Jing)

## 基于间断伽辽金法的悬停状态旋翼涡流场低耗散数值模拟

卞 威<sup>1</sup>, 招启军<sup>1</sup>, 赵国庆<sup>1,2</sup>

(1. 南京航空航天大学航空学院直升机旋翼动力学国家级重点实验室, 南京 210016, 中国;

2. 中国空气动力研究与发展中心旋翼空气动力学重点实验室, 绵阳 621000, 中国)

**摘要:** 建立间断伽辽金方法并将其应用于直升机旋翼桨尖涡演化和气动特性的精确模拟。首先, 选取旋转参考坐标系下的雷诺平均 N-S 方程作为控制方程, 采用嵌套网格方法对旋翼流场进行模拟, 在桨叶网格和背景网格上分别采用有限体积法和间断伽辽金法。此外, 空间离散采用高分辨率、低耗散的 Harten-Lax-Van Leer contact (HLLC) 格式, 时间离散采用显式三阶龙格-库塔格式。然后, 采用所建立的 CFD 方法对 C-T 旋翼的气动特性和桨尖涡演化进行了数值模拟, 计算结果与试验数据吻合较好, 很好地验证了间断伽辽金方法的准确性, 展示了其相较于有限体积方法在捕捉桨尖涡细节方面的优势。最后, 对比分析了在不同桨尖马赫数和旋翼总距下旋翼桨尖涡的演化规律。

**关键词:** 桨尖涡; 间断伽辽金法; N-S 方程; 气动特性; 直升机旋翼